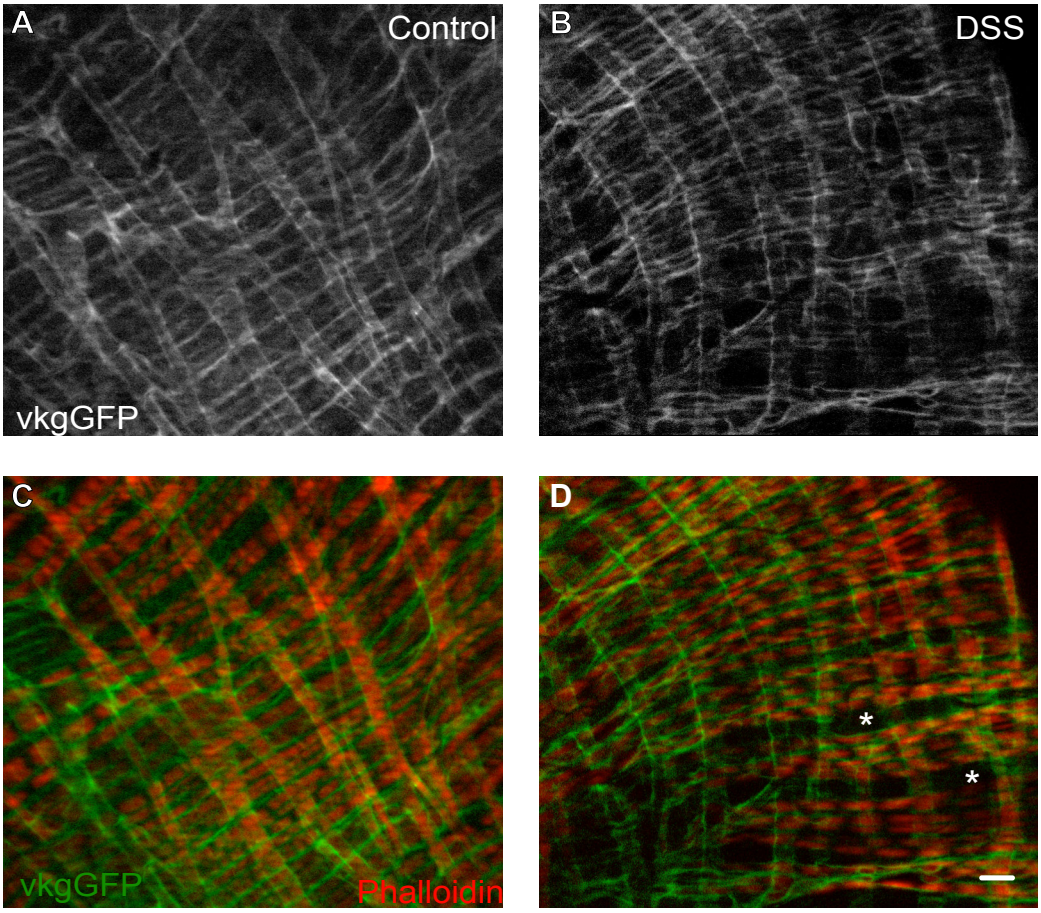

Fig. S1. Surface view of the gut basement membrane after DSS feeding.

(A) Tangential view of the gut basement membrane (Vkg-GFP) in control-fed flies. **(B)** Tangential view of gut basement membrane in DSS-fed flies. **(C-D)** Merged images of above showing the basement membrane (green) surrounding the muscles (phalloidin, red). Apparent "holes" in basement membrane (asterisks in D) represent areas where the muscles have separated. Scale bar= 10 μm.

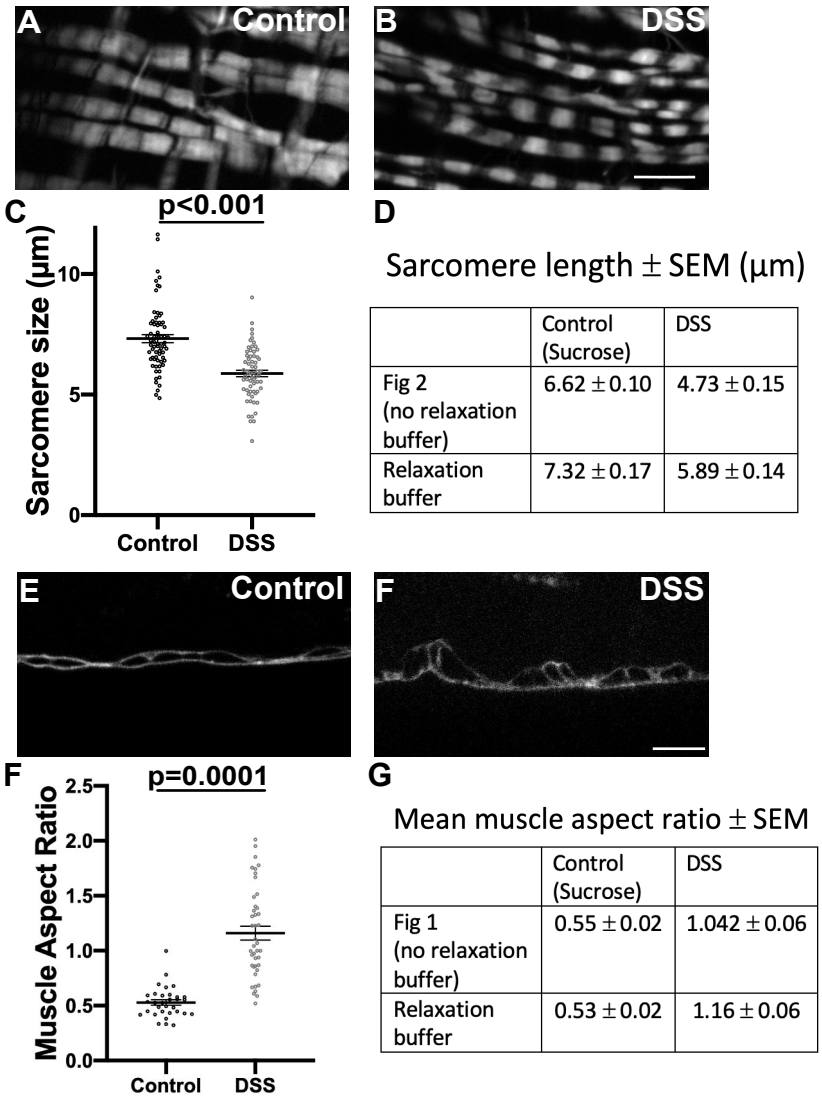

	Control (Sucrose)	DSS
Fig 2 (no relaxation buffer)	6.62 ± 0.10	4.73 ± 0.15
Relaxation buffer	7.32 ± 0.17	5.89 ± 0.14

	Control (Sucrose)	DSS
Fig 1 (no relaxation buffer)	0.55 ± 0.02	1.042 ± 0.06
Relaxation buffer	0.53 ± 0.02	1.16 ± 0.06

Fig. S2. DSS muscle damage is still evident when guts are treated with relaxing buffer.

Midguts from DSS-fed and control flies were dissected and incubated in relaxing buffer to allow muscle relaxation before analysis.

(A-B) Phalloidin staining to show sarcomeres in midgut longitudinal muscles dissected in relaxing buffer. **(C)** Sarcomere length is still significantly shorter in DSS fed flies than control-fed flies, indicating that muscles are damaged and not simply contracted by DSS. **(D)** Relaxing buffer did cause moderate lengthening of sarcomeres in both control and DSS fed flies when compared to sarcomere sizes from Fig. 2.

(E-F) Vkg-GFP outlines were used to calculate the cirumferential muscle aspect ratio of guts treated with relaxing buffer. (**G)** Muscle aspect ratio is still significantly greater in DSS fed flies than control fed flies, indicating that muscles are damaged and not simply contracted by DSS. (**H)** Relaxation buffer had little effect on the aspect ratio

Scale bars = 10 µm

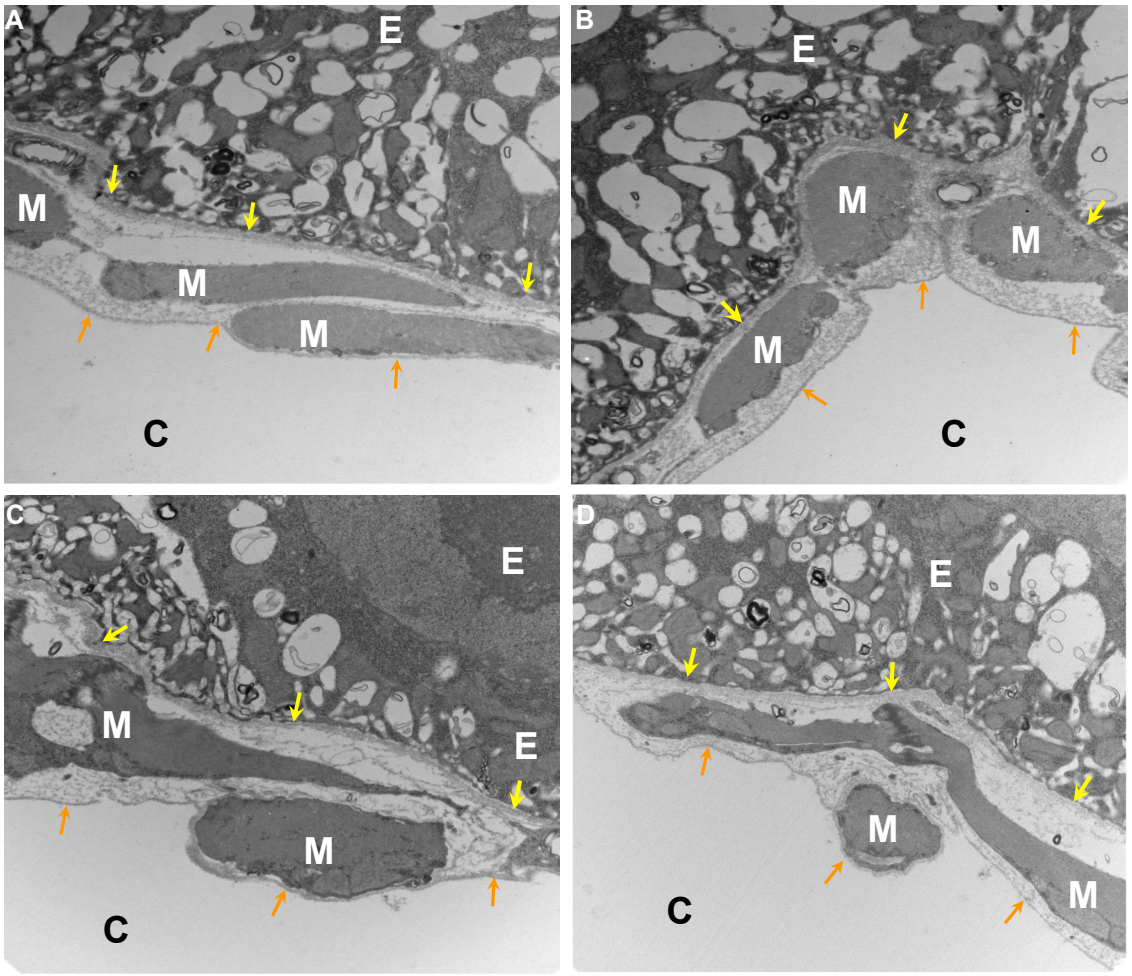

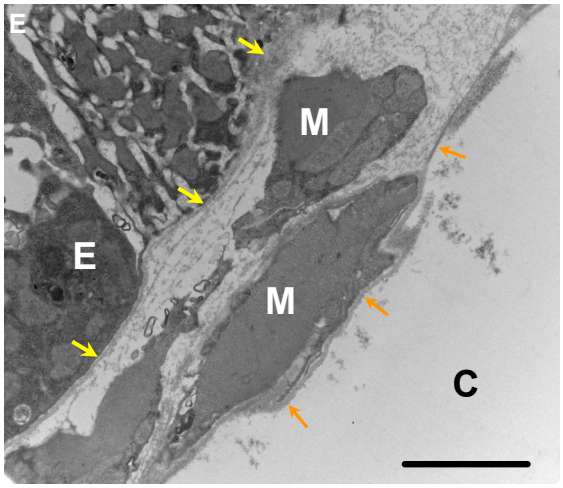

E- enterocyte epithelial layer.

C- body cavity.

M - muscle.

Scale bar = 2 μm

Fig. S3. The basement membranes of control midguts show a variety of morphologies.

A-E. TEM images of control wild-type (w^{1118}) midguts, fed 48 h on a sucrose diet. The longitudinal and circumferential muscles are perpendicularly oriented to each other. In TEM images, the longitudinal muscles appear round in cross-section, whereas circumferential muscles appear long, because guts were cut in cross-section. In contrast, SIM and optical sections are taken along the long axis, so that the circumferential mucles appear round and longitudinal muscles appear long as shown in Fig. 1A. Either circumferential or longitudinal muscles can be found next to the body cavity (see also Figs. 3A and 5B), leading us to conclude that the longitudinal and circumferential muscles are in some kind of basket weave pattern, as depicted in Fig. 1A.

Sheet-like basement membranes are observed 1) underneath the epithelial enterocyte layer, indicated by yellow arrows, and 2) outside the muscles separating them from the body cavity, indicated by orange arrows. The structure of the material between these two layers is unclear, although SIM imaging indicates that the material between and around the muscles contains collagen IV even though it is not organized into a sheet (Figs. 3D and 7A).

Journal of Cell Science • Supplementary information

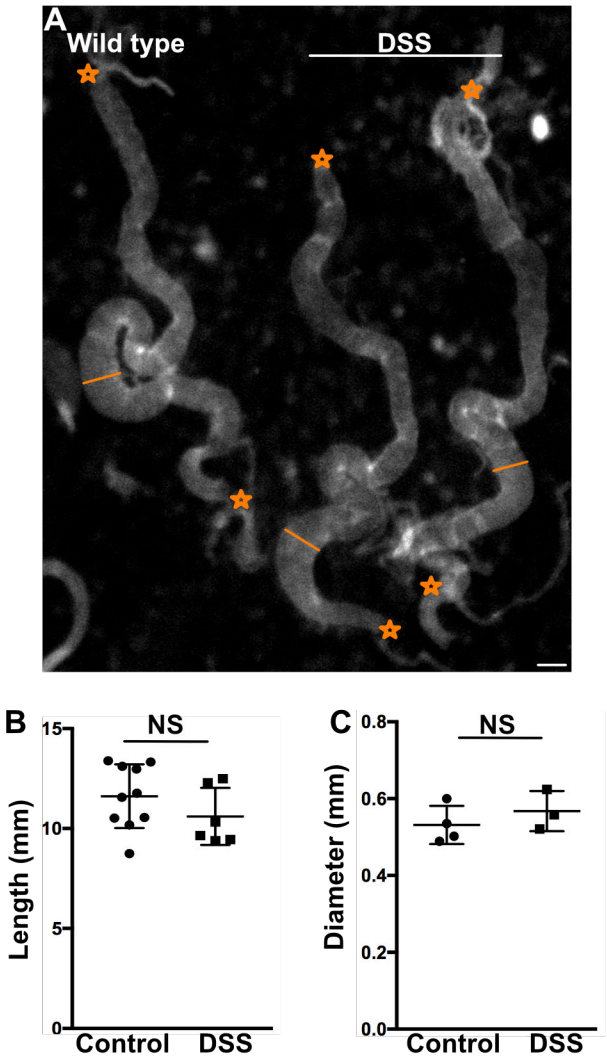

Fig. S4. DSS has no significant effect on the length or diameter of the gut.

(A) Brightfield image of guts dissected from control flies. The entire gut length is measured as the distance between the two stars, top and bottom. The diameter is measured as indicated by the orange line across the midgut. **(B-C)** Neither the length (B) or diameter (C) was significantly changed between animals fed DSS vs control food for 48 h. Scale bar = 500 μm

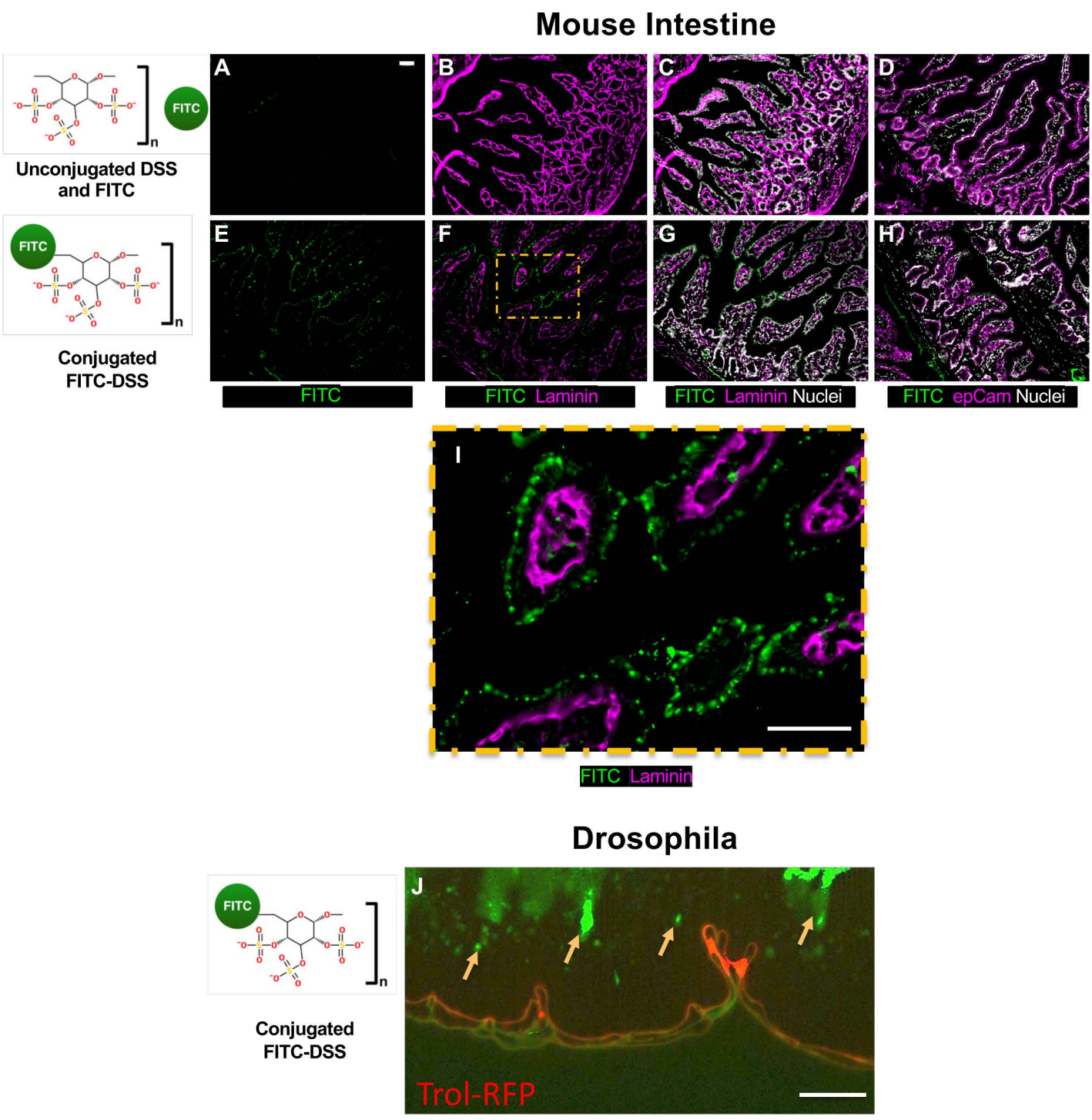

Fig. S5. In mice, DSS does not accumulate in intestinal basement membranes but rather at cellular junctions.

(A-D) Intestines from control mice administered DSS and unconjugated FITC. (A-C) represent the same sample stained for the basement membrane protein laminin, whereas (D) was stained for E-cadherin. No clear FITC signal is observed (A).

(E-H) Intestines from mice administered FITC-DSS. (E-G) represent the same sample stained for the basement membrane protein laminin, whereas (H) was stained for E-cadherin. FITC-DSS localized in punctae (E) that did not colocalize with laminin. Rather, FITC-DSS localized near the epithelial plasma membrane, stained with E-Cadherin (H). **(I)** A magnified region of F showing FITC-DSS does not co-localize with the basement membrane. Scale bar= 50 μm.

(J) Drosophila guts with FITC-DSS evident in the enterocytes, likely during transport. The lumen is omitted from the top of the image because it is significantly brighter. Scale bar = 10 μm.

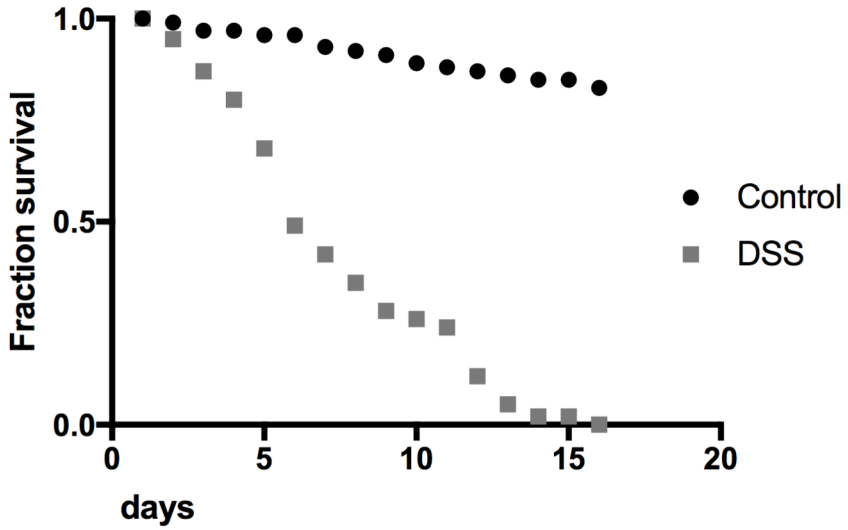

Fig. S6. Flies fed DSS have an increased mortality rate.

Flies continuously fed DSS for 16 days die rapidly compared to controls. These results are similar to those reported by Amcheslavsky et al (2009).

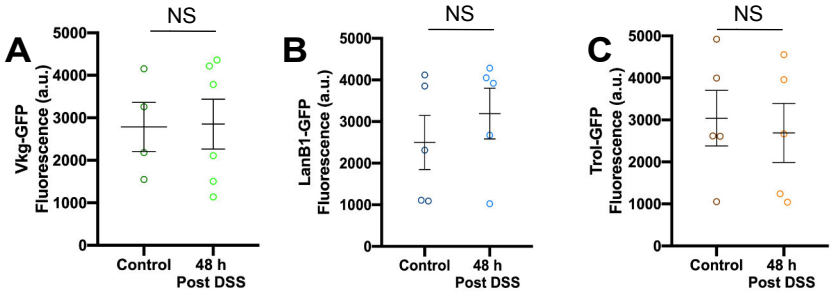

Fig. S7. Basement membrane protein levels were not significantly different after repair.

(A-C) Basement membrane protein levels were not significantly different in control vs. DSS-fed midguts allowed to recover for 48 h, as indicated by fluorescence levels of Vkg-GFP (A), LanB1-GFP (B) or Trol-GFP (C). Fluorescence was measured 48 h after removal from DSS to normal food; controls were sucrose-fed for 48 h then switched to normal food for 48 h to match experimental conditions. Each dot represents one gut.

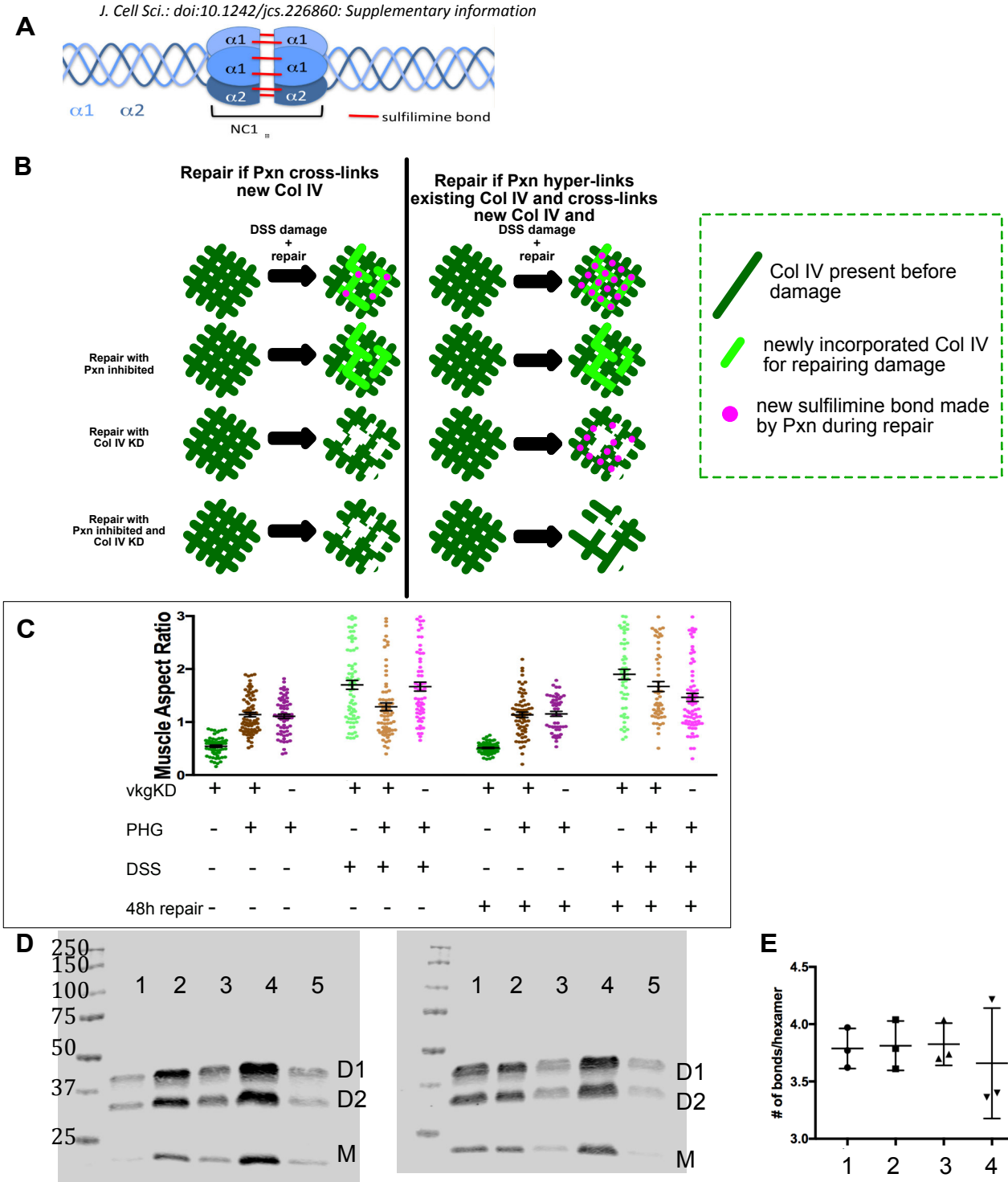

Fig. S8. Peroxidasin does not hypercrosslink basement membrane during repair.

(A) Schematic showing 6 possible sulfilimine bonds per NC1 hexamer. **(B)** Models illustrate how loss of both collagen IV and Pxn are expected to affect repairing basement membrane: (left) Pxn is required only to crosslink the newly inserted collagen IV; (right) Pxn hypercrosslinks the basement membrane to stabilize it as part of the repair process. **(C)** Muscle aspect ratios after *vkg* knockdown (with *TubP-Gal4, Gal80ts*), Pxn inhbition by PHG, or both treatments, after control or DSS feeding, with or without a repair period of 48h after DSS withdrawal. Because the double treatment is not worse than the single treatments, we conclude that Pxn does not hypercrosslink collagen IV during repair. **(D)** 2 western blots of gut samples showing the Collagen IV NC1 domain, which has altered electrophoretic mobility depending on its crosslinked status: D1 is a dimer with one sulfilimine crosslink, D2 is dimer with two sulfilimine crosslinks, and M is monomer without crosslinks. Lanes: 1-normal food, 2-sucrose, 3-DSS no recovery, 4-DSS 48 h recovery, and 5-PHG. **(E)** The number of sulfilimine bonds calculated per hexamer of the 5 different condition types in 3 biological replicates. Sulfilimine crosslinking does not increase either after DSS treatment or repair.

Table S1. Statistics on Figure 7G*

Samples compared	P value†
Sibling Control	
A-B (0 h v 48 h, sucrose)	ns
A-C (0 h sucrose v 0 h DSS)	<0.001
B-D (48 h sucrose v 48 h DSS)	ns
C-D (0 h v 48 h, DSS)	<0.001
Pxn-KD	
E-F (0 h v 48 h, sucrose)	0.007
E-G (0 h sucrose v 0 h DSS)	<0.001
F-H (48 h sucrose v 48 h DSS)	<0.001
G-H (0 h v 48 h, DSS)	ns

* Columns in Figure 7G are lettered alphabetically left to right
† ANOVA with unpaired t-tests with a Bonferroni correction

Table S2. Statistics on Figure 7N*

Samples compared	P value†
Sibling Control	
A-B (0 h v 48 h, sucrose)	ns
A-C (0 h sucrose v 0 h DSS)	<0.001
B-D (48 h sucrose v 48 h DSS)	ns
C-D (0 h v 48 h, DSS)	<0.001
Pxn-KD	
E-F (0 h v 48 h, sucrose)	ns
E-G (0 h sucrose v 0 h DSS)	<0.001
F-H (48 h sucrose v 48 h DSS)	<0.001
G-H (0 h v 48 h, DSS)	ns
PHG	
I-J (0 h v 48 h, sucrose)	0.04
I-K (0 h sucrose v 0 h DSS)	<0.001
J-L (48 h sucrose v 48 h DSS)	<0.001
K-L (0 h v 48 h, DSS)	<0.001

* Columns in Figure 7N are lettered alphabetically left to right
† ANOVA with unpaired t-tests with a Bonferroni correction

Table S3. Statistics on Figure 8J*

Samples compared	P value†
Sibling Control	
A-B (0 h v 48 h, sucrose)	ns
A-C (0 h sucrose v 0 h DSS)	<0.001
B-D (48 h sucrose v 48 h DSS)	ns
C-D (0 h v 48 h DSS)	<0.001
Vkg-KD	
E-F (0 h v 48 h, sucrose)	ns
E-G (0 h sucrose v 0 h DSS)	<0.001
F-H (48 h sucrose v 48 h DSS)	<0.001
G-H (0 h v 48 h, DSS)	0.001
LanB1-KD	
I-J (0 h v 48 h, sucrose)	ns
I-K (0 h sucrose v 0 h DSS)	<0.001
J-L (48 h sucrose v 48 h DSS)	<0.001
K-L (0 h v 48 h, DSS)	ns

* Columns in Figure 8J are lettered alphabetically left to right
† ANOVA with unpaired t-tests with a Bonferroni correction

Table S4. Drosophila lines used in this study.

Genotype	Source	Used for
w^{1118}	Todd Laverty, Janelia Farm	Figs. 2, 3, 4, 5, 6, S2, S3, S4, S6
w; vkg-GFP^{454}	Yale Flytrap Project	Figs. 1, 3, 7, 8, S1, S2, S7, S8
w; LanB1-GFP	VDRC 318180	Figs. 1, 3, S7
trol-GFP^{1700} *w*	Flytrap line ZCL1973	Figs. 1, 3, S7
y trol-RFP w	Vincent Mirouse, French National Centre for Scientific Research	Figs. 4, S5
w; UAS-vkg^{RNAi}	VDRC 106812	Figs. 8, S8
w; UAS-vkg^{RNAi}	VDRC 41278	Not shown
w; *UAS-LanB1*^{RNAi}	VDRC 23121	Figs. 2, 8
w; *UAS-LanB1*^{RNAi}	VDRC 23119	Not shown
w; vkg-GFP^{454}*/CyO; UAS-Pxn*^{RNAi} */ TubP-Gal4, TubP-Gal80*^{ts}	This study; VDRC 15276	Figs. 1, 7
w UAS- Pxn^{RNAi}/FM7c	VDRC 15277	Not shown
w; *vkg-GFP*^{205}; *TubP-Gal4*, *TubP-Gal80*^{ts}*/SM6-TM6B*	Ramos-Lewis et. al. 2018	Fig. 8
w; *LanB1-GFP TubGal4 TubP-Gal80*^{ts}*/TM6B*	Ramos-Lewis et. al. 2018	Figs. 8, S8